Optics Letters

Al_2O_3:Yb^{3+} integrated microdisk laser label-free biosensor

Michiel de Goede,[1] Lantian Chang,[1] Jinfeng Mu,[1] Meindert Dijkstra,[1] Raquel Obregón,[2] Elena Martínez,[2,3,4] Laura Padilla,[5] Francesc Mitjans,[5] and Sonia M. Garcia-Blanco[1,*]

[1]Optical Sciences Group, MESA+ Institute for Nanotechnology, University of Twente, P.O. Box 217, 7500 AE Enschede, The Netherlands
[2]Institute for Bioengineering of Catalonia, The Barcelona Institute of Science and Technology, Baldiri Reixac 10-12, 08028 Barcelona, Spain
[3]Department of Electronics and Biomedical Engineering, University of Barcelona, Barcelona 08028, Spain
[4]Centro de Investigación Biomédica en Red, Madrid 28029, Spain
[5]Health & Biomedicine unit of LEITAT Technological Center, Barcelona Science Park, Barcelona 08028, Spain
*Corresponding author: s.m.garciablanco@utwente.nl

Received 23 August 2019; revised 24 October 2019; accepted 24 October 2019; posted 24 October 2019 (Doc. ID 376128); published 5 December 2019

Whispering gallery mode resonator lasers hold the promise of an ultralow intrinsic limit of detection. However, the widespread use of these devices for biosensing applications has been hindered by the complexity and lack of robustness of the proposed configurations. In this work, we demonstrate biosensing with an integrated microdisk laser. Al_2O_3 doped with Yb^{3+} was utilized because of its low optical losses as well as its emission in the range 1020–1050 nm, outside the absorption band of water. Single-mode laser emission was obtained at a wavelength of 1024 nm with a linewidth of 250 kHz while the microdisk cavity was submerged in water. A limit of detection of 300 pM (3.6 ng/ml) of the protein rhS100A4 in urine was experimentally demonstrated, showing the potential of the proposed devices for biosensing.

https://doi.org/10.1364/OL.44.005937

Passive microresonator optical sensors have been widely studied in last decades for their high sensitivity in the label-free detection of biomolecules [1–3]. These biosensors hold promise for their integration into portable, sensitive, low-cost, multiplexed, and easy-to-use devices that, within minutes, can detect biomarkers from bodily fluids for medical applications. Label-free detection relies on the sensitivity of the microresonators to changes in their local environment (i.e., evanescent field) due to the attachment of the target biomolecules, which, among other effects, induces shifts in the resonance frequency [4]. Such biosensors exhibit an intrinsic resolution limit given by the linewidth of the resonances [5], and require complex interrogation schemes with either tunable lasers or high-resolution optical spectrum analyzers (OSA) to continuously monitor the location of the resonance wavelength, which hampers their implementation outside the laboratory.

In contrast to passive resonators, recent reports highlight the potential advantages of active, laser-based devices [6–12]. The much narrower resonances of microresonator lasers dramatically decreases the intrinsic limit of detection (LOD). Furthermore, a simple, low-cost interrogation setup can be used to monitor the laser wavelength shift by heterodyning with an external reference laser [13]. However, up to date, the benefits attributed to active, laser-based devices have been mostly demonstrated on complicated three-dimensional optical cavities not suitable for on-chip integration, therefore hampering their widespread use as multiplexed biosensing platforms. Advancing sensing functionalities based on active microresonators requires a material platform that can overcome this limitation.

Aluminum oxide (Al_2O_3) is an emerging photonic material that exhibits a large transparency window covering the visible and near-infrared wavelength ranges [14]. When doped with rare-Earth ions, it provides optical gain that has been used to demonstrate on-chip amplifiers [15] and lasers [16,17]. Recent reports have shown its monolithic integration with passive photonic functions [18–20]. These features make this material very interesting for the realization of active optical sensors. In particular, doping Al_2O_3 with Yb^{3+} permits operation at a wavelength of ~1000 nm, where water absorption is negligible. To date, there is only one report exploiting the active optical properties of Al_2O_3 as a sensing material, where glass microspheres (1 to 20 μm in diameter) were detected by using a dual-wavelength distributed feedback laser [21]. The detection was not selective, as the device was sensitive to any microsphere brought into its close proximity.

In this work, an Al_2O_3:Yb^{3+} integrated microdisk laser biosensor is developed for the label-free detection of the S100A4 protein (12 kDa), which has been associated with human tumor development [22,23]. Detection of a concentration as low as 300 pM of the S100A4 protein in synthetic urine is experimentally demonstrated. This falls within the concentration range being reported as clinically relevant [24], therefore showing the potential of this active platform for label-free biosensing.

Al_2O_3:Yb^{3+} films were first deposited by radio frequency (RF) reactive cosputtering (AJA ATC 1500) from Al and Yb

targets to form a 550 nm thick dielectric layer onto a thermally oxidized silicon wafer [25]. The substrate was heated to 450°C during the deposition. RF powers of 200 W and 35 W were applied to the Al and Yb targets, respectively. Oxygen and argon flows of 2.5 sccm and 30 sccm, respectively, were utilized with an operating pressure of 3.7 mTorr [25]. Microdisks and bus waveguides were patterned by UV contact lithography followed by reactive ion etching with BCl_3:HBr (5:2) using a total power of 25 W [26]. The microdisk has a radius of 100 μm and a coupling gap of 0.6 μm to the bus waveguide, which has a width of 1.4 μm. With these disk dimensions, a 6.5% overlap of the electric field with the environment (i.e., water or synthetic urine upper cladding) was calculated. A 3 μm thick SiO_2 cladding was deposited by plasma-enhanced chemical vapor deposition (Oxford Plasmalab 80 Plus) at 300 °C through a shadow mask to cover the input and output bus waveguides, leaving the microdisks fully exposed to the environment. Next, chips of 1.2×1.9 cm^2 were diced (Micro Ace 3). PDMS microfluidic channels with a cross section of 600 by 70 μm^2 were bonded onto the sample by simply placing them on top of the chip. Finally, the PDMS channels were filled with either deionized (DI) water (bulk refractive index and temperature sensitivity experiments) or synthetic urine (biosensing experiment).

Figure 1(a) shows the device under test on the experimental setup. During the measurements, the temperature of the chip is controlled to 21.5 ± 0.0025°C by means of a temperature-regulated stage. A fiber laser diode (Thorlabs BL976-SAG300) with a wavelength of 976 nm and linewidth of 0.5 nm is used to optically pump the Al_2O_3:Yb^{3+} microdisk lasers. The backward lasing light (TE polarized) is separated from the residual pump with a 980/1060 nm wavelength demultiplexer (Thorlabs WD202G-FC) and analyzed with a Hewlett Packard 70950B OSA while its power is measured with a Hewlett Packard 81536 A power sensor. The emission spectrum

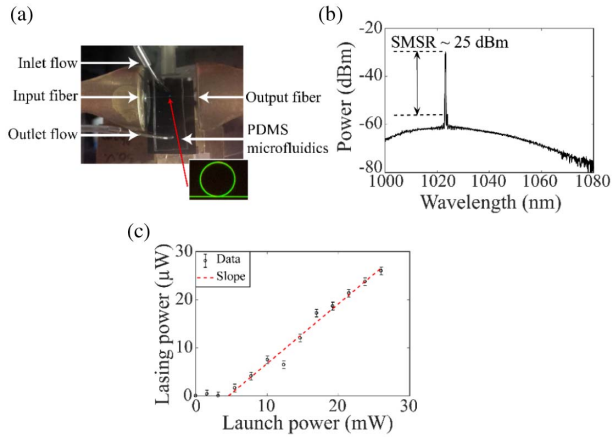

Fig. 1. (a) Photograph of the optofluidic chip on the experimental setup. Both input and output fibers aligned to the sensor chip are shown as well as the inlet/outlet to the microfluidic channel. The inset shows the Al_2O_3:Yb^{3+} microdisk laser under pump illumination (976 nm). The green luminescence originates from upconversion of Er^{3+} ion impurities in the microdisk. (b) Lasing spectrum of the microdisk laser with a DI water cladding at a launched pump power of 27 mW at 976 nm. Spectral resolution is 100 pm. (c) Power characteristics of the laser, which has a slope efficiency of 0.1% and a threshold of 7 mW.

of the device subject to a flow of DI water is shown in Fig. 1(b), measured with a resolution of 100 pm. Single-mode operation at 1024 nm with a side-mode suppression ratio (SMSR) of 27 dBm is observed. The laser operates in TE polarization. A slope efficiency (i.e., laser power measured at the power meter with respect to launched pump power prior to coupling to the chip) of ~0.1% and a lasing threshold of 7 mW launched pump power prior to coupling to the chip are measured. Currently, these power characteristics are limited by the low fiber-to-chip coupling efficiency of 20%, which could be enhanced in future works by implementing a vertical tapered end facet for higher fiber-to-chip coupling efficiency, and thus, larger slope efficiency and lower lasing threshold. Furthermore, the passive resonances of the disk resonator were scanned around the lasing wavelength with a tunable laser (10 kHz TOPTICA CTL 1050). It was found that at the lasing wavelength, the device has a cold quality factor of 1.2×10^5 and is undercoupled. Increasing the coupling coefficient to achieve critical coupling at the pump wavelength could also be beneficial for the lasing performance due to an increase of the enhancement factor of the pump light circulating in the disk resonator.

The emission spectrum of the single-mode microdisk laser is heterodyned with the same tunable laser emitting at an almost identical wavelength [Fig. 2(a)] to achieve a low-frequency heterodyne beatnote (i.e., below 10 GHz) detectable by a RF spectrum analyzer (Hewlett Packard E4407B) [13]. The frequency of the beatnote, f_{beat}, is given by

$$f_{beat} = c\frac{\lambda_2 - \lambda_1}{\lambda_1 \lambda_2}, \tag{1}$$

with c being the speed of light in vacuum, and λ_1 and λ_2 being the wavelengths of the Al_2O_3:Yb^{3+} microdisk laser and of the external reference laser, respectively. The beatnote spectrum can be seen in Fig. 2(b), containing two closely separated RF peaks, which are due to the splitting of the microdisk lasing mode due to the coupling between the clockwise (CW) and counterclockwise (CCW) propagating modes in the disk [27]. Both peaks of the RF beatnote shift due to environmental perturbations applied to the microdisk. The laser linewidth of the Al_2O_3:Yb^{3+} microdisk laser is determined from the linewidth of the heterodyne beatnotes in the RF spectrum to be ~200–300 kHz [28]. A direct self-beating spectrum between the CW and CCW laser modes exhibits a 3 dB linewidth of ~500 kHz (RF spectral resolution of 100 kHz, 50 ms measurement time), which confirms a laser linewidth of ~250 kHz for each of the laser split modes, which corresponds to a quality factor of $\sim 1 \times 10^9$.

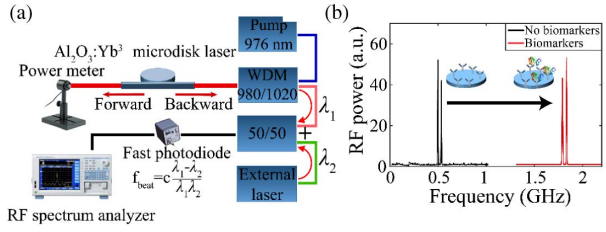

Fig. 2. (a) Schematic of the heterodyne detection for monitoring the change of the microdisk laser frequency. (b) RF beatnote between the microdisk laser and the external laser during a flow of synthetic urine (black curve) and synthetic urine spiked with rhS100A4 at a concentration of 30 nM (red curve).

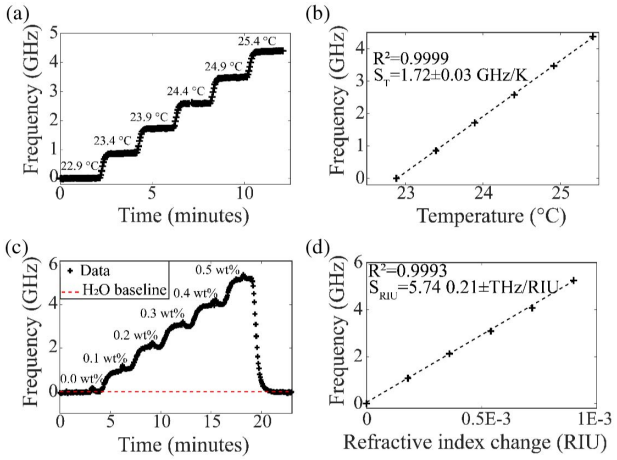

Fig. 3. Bulk sensing characterization. (a) Beatnote frequency (between the lower frequency laser peak and the external laser) as a function of time for different chip holder temperatures. DI water was flown through the microfluidic channel during the experiment at a flow rate of 10 μl/min. (b) Temperature slope sensitivity. The dotted line is a linear fit. (c) Beatnote frequency as a function of time as different concentrations of NaCl in DI water (0.0–0.5 wt. %) are flown over the microdisk laser sensor in time steps of 3 min with a flow rate of 30 μl/min. (d) Bulk refractive index slope sensitivity. The dotted line is a linear fit.

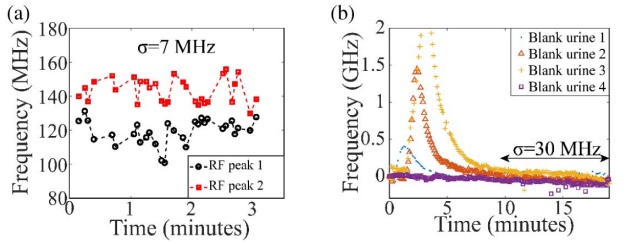

Fig. 4. (a) Beatnote frequency between both laser modes and the external laser during 3 min of DI water flow. A frequency noise of 7 MHz was determined. (b) Beatnote frequency of the lower laser mode during a 20 min flow of synthetic urine. Four experiments were carried out. The increase in the beatnote frequency at about 1 to 4 min results from the short-time temperature overshoot caused by the introduction of the urine samples. The beatnote frequency returns to the baseline after the overshoot. The frequency noise was determined during the last 10 min of the measurement to be ~30 MHz.

The temperature and bulk refractive index sensitivity of the microdisk laser are characterized (Fig. 3). The beatnote frequency between the lower frequency laser peak of the microdisk laser and the external laser is monitored while varying the temperature of the device from room temperature to 25.4°C in steps of 0.5°C. During the measurements, 15 RF spectra per minute are recorded at a resolution of 1 MHz. A temperature sensitivity of 1.72 ± 0.03 GHz/K (6.02 ± 0.11 pm/K) is obtained, which is much smaller than the temperature sensitivity of Si microring resonators [29]. The bulk refractive index sensitivity is characterized by flowing water solutions of different concentrations of NaCl (0.0–0.5 wt. %) through the microfluidic channel. A bulk refractive index sensitivity of 5.74 ± 0.21 THz/RIU (20.1 ± 0.7 nm/RIU) is obtained, similar to the sensitivity reported earlier for a passive Al_2O_3 microring resonator [30]. Both peaks in the RF spectrum have identical sensitivities. The sensitivity is not very high compared with conventional, silicon-on-insulator microring resonators [4], because the disk resonator has a rather high confinement and low fraction of optical power circulating in the analyte medium. Using a microring resonator or a thinner microdisk resonator could increase the sensitivity, although this could negatively affect the lasing performance by inefficient absorption of pump light. The LOD of the sensor is the smallest bulk refractive index variation that can be reliably detected (i.e., three times the standard deviation of the noise [5]). To determine the noise, the RF beatnote is recorded for 3 min while DI water is flown through the microfluidic channel on top of the sensor [Fig. 4(a)]. Both RF peaks exhibit the same noise, $\sigma = 7$ MHz (i.e., 24 fm). The noise arises mainly from fluctuations of the temperature of the chip, of the power of the laser diode used for pumping, and of the microfluidic flow (i.e., mainly refractive index and temperature fluctuations). A further source of noise is the fluctuation of the frequency of the external laser due to temperature or atmospheric pressure variations within the laser cavity. A LOD of 3.7×10^{-6} RIU can be extracted from these measurements. This LOD is similar to previous reports on passive microring resonator sensors, due to the sensor being currently limited by its noise and therefore not benefiting yet from the much smaller intrinsic LOD of 5×10^{-8} RIU achieved in this active sensor (i.e., due to the increase in the Q-factor by about three orders of magnitude with respect to a passive microdisk). Fully exploiting the benefits of the narrow linewidth, and the high intrinsic LOD, of the active microdisk would require eliminating the noise sources present in the current system.

Finally, the microdisk laser is used to detect rhS100A4 proteins present in known concentrations using synthetic urine as a model of a complex body fluid. Molecular recognition based on highly specific protein–antibody reactions is used for the biosensing. To that end, monoclonal antibodies, which are able to bind rhS100A4, are immobilized onto the surface of the microdisks using the approach suitable for Al_2O_3:Yb^{3+} surfaces previously designed by us [30]. In order to determine the noise during biosensing experiments, samples of synthetic urine (SurineTM Negative Urine Control, Sigma Aldrich) are flown over the microdisk laser at a flow rate of 40 μl/min [Fig. 4(b)]. An increase of the beatnote frequency can be observed during the initial 1 to 4 min after the introduction of the urine, due to temperature fluctuations. An average noise of $\sigma = 30$ MHz is determined over the last 10 min; in the protein experiments, this figure was $\sigma = 25$ MHz. Synthetic urine spiked with increasing concentrations of the rhS100A4 protein, ranging from 100 pM to 3 μM, is then flown over the sensor. The evolution of the RF spectra due to the binding of proteins to the immobilized antibodies is recorded for 20 min per concentration. Figure 5 shows the shift of the lowest frequency RF beatnote peak as a function of time for different protein concentrations. For all of them, a positive shift of the RF frequency occurs. This signal flattens over time, indicating that a dynamic equilibrium between binding and disassociation of the proteins to the antibodies is reached. Furthermore, the total amount of frequency shift after 20 min increases with the protein concentration. The lowest detected rhS100A4 protein concentration

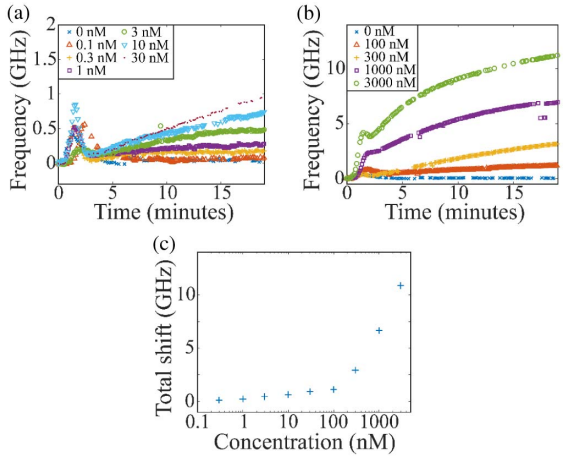

Fig. 5. Beatnote frequency changes due to binding of the rhS100A4 protein to the antibodies immobilized onto the microdisk laser. The samples were flown at a rate of 40 μl/min for 20 min. The initial bumps at around 1 to 2 min are results of a short-time temperature overshoot caused by the dynamics of the flow system. (a) Data of low protein concentrations. (b) Data of high protein concentrations. (c) Biosensor calibration curve.

in synthetic urine is 300 pM, for which a frequency shift of 162 ± 13 MHz is recorded, which exceeds three times the noise in blank synthetic urine samples (90 MHz). This result represents one of the lowest concentrations reported in the literature for the label-free detection in a complex matrix (i.e., synthetic urine), and it is 1 order of magnitude lower than the LOD that we achieved for the same protein using a passive ring resonator sensor [30]. However, as discussed above, this limit is still far from the intrinsic LOD derived by the laser linewidth. This result shows the possibility of using an active disk resonator to detect a clinically relevant cancer biomarker from a complex liquid, such as urine, at low LOD.

To conclude, in this work, we report the first proof of concept of the label-free biosensing capabilities of active, laser-based sensors based on Al_2O_3:Yb^{3+} microdisk resonators. The microdisks lasers can be integrated on-chip and, combined with microfluidics, exhibit narrow-linewidth single-mode lasing while operating in an aqueous environment. A heterodyning detection scheme using an external reference laser operating at a wavelength very close to the emission wavelength of the microdisk was used. A bulk refractive index sensitivity and LOD comparable with the state-of-the-art passive sensors was achieved, but with the advantage of using a simple, (potentially) portable, and low-cost readout scheme. Upon the stable binding of antibodies, the specific molecular recognition of rhS100A4 proteins, associated to cancer development, in synthetic urine was demonstrated. Detection of concentrations as low as 300 pM shows the biosensing capabilities of the Al_2O_3:Yb^{3+} microdisk resonators. These results pave the road towards the realization of biosensing platforms based on active, laser-based devices easy to integrate in point-of-care instruments equipped with portable, simple, and relatively cheap readout schemes.

Funding. European Union's Horizon 2020 Framework Programme (634928); CERCA Programme/Generalitat de Catalunya (2017-SGR-1079); Spanish Ministry of Economy and Competitiveness (Severo Ochoa Program for Centers of Excellence in R&D 2016-2019).

Acknowledgment. The results presented here reflect only the views of the authors; the European Commission is not responsible for any use that may be made of the information it contains.

Disclosures. The authors declare no conflicts of interest.

REFERENCES

1. J. Su, Sensors **17**, 540 (2017).
2. X. Fan, I. M. White, S. I. Shopova, H. Zhu, J. D. Suter, and Y. Sun, Anal. Chim. Acta **620**, 8 (2008).
3. E. Kim, M. D. Baaske, and F. Vollmer, Lab Chip **17**, 1190 (2017).
4. P. Steglich, M. Hülsemann, B. Dietzel, and A. Mai, Molecules **24**, 519 (2019).
5. I. M. White and X. Fan, Opt. Express **16**, 1020 (2008).
6. T. Reynolds, N. Riesen, A. Meldrum, X. Fan, J. M. M. Hall, T. M. Monro, and A. François, Laser Photon. Rev. **11**, 1600265 (2017).
7. X. Zhang, L. Ren, X. Wu, H. Li, L. Liu, and L. Xu, Opt. Express **19**, 22242 (2011).
8. J. Yang and L. J. Guo, IEEE J. Sel. Top. Quantum Electron. **12**, 143 (2006).
9. A. Meldrum, W. Morrish, S. Lane, W. Wu, T. M. Monro, and A. François, Phys. Status Solidi A **215**, 1700619 (2018).
10. L. Ren, X. Zhang, X. Guo, H. Wang, and X. Wu, IEEE Photon. Technol. Lett. **29**, 639 (2017).
11. W. Morrish, N. Riesen, S. Stobie, A. François, and A. Meldrum, Phys. Rev. Appl. **10**, 051001 (2018).
12. S. Lozenko, D. Faye, H. Zhang, M. Lebental, J. Lautru, J. Zyss, J. P. Lefevre, and I. Leray, Appl. Phys. B **117**, 501 (2014).
13. A. J. Maker and A. M. Armani, Appl. Phys. Lett. **103**, 123302 (2013).
14. G. N. West, W. Loh, D. Kharas, C. Sorace-Agaskar, K. K. Mehta, J. Sage, J. Chiaverini, and R. J. Ram, APL Photon. **4**, 026101 (2019).
15. S. A. Vázquez-Córdova, M. Dijkstra, E. H. Bernhardi, F. Ay, K. Wörhoff, J. L. Herek, S. M. García-Blanco, and M. Pollnau, Opt. Express **22**, 25993 (2014).
16. E. H. Bernhardi, H. A. G. M. Van Wolferen, K. Wörhoff, R. M. De Ridder, and M. Pollnau, Opt. Lett. **36**, 603 (2011).
17. J. D. B. Bradley, E. S. Hosseini, Z. Su, T. N. Adam, G. Leake, D. Coolbaugh, and M. R. Watts, Opt. Express **22**, 12226 (2014).
18. C. I. Emmerik, M. Dijkstra, M. de Goede, L. Chang, J. Mu, and S. M. García-Blanco, Opt. Mater. Express **8**, 3049 (2018).
19. J. Mu, M. Dijkstra, Y. S. Yong, M. de Goede, L. Chang, and S. M. G. Blanco, IEEE J. Sel. Top. Quantum Electron. **25**, 8200911 (2019).
20. M. Pollnau and J. D. B. Bradley, Opt. Express **26**, 24164 (2018).
21. E. H. Bernhardi, K. O. van der Werf, A. J. F. Hollink, K. Wörhoff, R. M. de Ridder, V. Subramaniam, and M. Pollnau, Laser Photon. Rev. **7**, 589 (2013).
22. S. K. Mishra, H. R. Siddique, and M. Saleem, Cancer Metastasis Rev. **31**, 163 (2012).
23. B. R. Davies, M. O'Donnell, G. C. Durkan, P. S. Rudland, R. Barraclough, D. E. Neal, and J. K. Mellon, J. Pathol. **196**, 292 (2002).
24. J. L. Turnier, N. Fall, S. Thornton, D. Witte, M. R. Bennett, S. Appenzeller, M. S. Klein-Gitelman, A. A. Grom, and H. I. Brunner, Arthritis Res. Ther. **19**, 242 (2017).
25. K. Worhoff, J. D. B. Bradley, F. Ay, D. Geskus, T. P. Blauwendraat, and M. Pollnau, IEEE J. Quantum Electron. **45**, 454 (2009).
26. J. D. B. Bradley, F. Ay, K. Wörhoff, and M. Pollnau, Appl. Phys. B **89**, 311 (2007).
27. D. S. Weiss, V. Sandoghdar, J. Hare, V. Lefèvre-Seguin, J.-M. Raimond, and S. Haroche, Opt. Lett. **20**, 1835 (1995).
28. T. Okoshi, K. Kikuchi, and A. Nakayama, Electron. Lett. **16**, 630 (1980).
29. B. Guha, B. B. C. Kyotoku, and M. Lipson, Opt. Express **18**, 3487 (2010).
30. M. de Goede, M. Dijkstra, R. Obregón, J. Ramón-Azcón, E. Martínez, L. Padilla, F. Mitjans, and S. García-Blanco, Opt. Express **27**, 18508 (2019).